CLUSTERS AND SUPERCLUSTERS IN THE SLOAN AND LAS CAMPANAS SURVEYS

J. EINASTO

Tartu Observatory, EE-61602 Tõravere, Estonia

We generate the 2-dimensional high-resolution density field of galaxies of the Early Data Release of the Sloan Digital Sky Survey and the Las Campanas Redshift Survey with a smoothing length 0.8 h^{-1} Mpc to extract clusters and groups of galaxies, and a low-resolution field with a smoothing length 10 h^{-1} Mpc to extract superclusters of galaxies. We investigate properties of density field clusters and superclusters and compare the properties of these clusters and superclusters with those of Abell clusters, and superclusters found on the basis of Abell clusters. We found that clusters in a high-density environment have a luminosity a factor of $5 - 10$ higher than in a low-density environment. Clusters and superclusters in the Northern slice of SDSS are much richer than those in the Southern slice.

1. Introduction

Clusters and groups of galaxies are the basic building blocks of the Universe on cosmological scales. The first catalogues of clusters of galaxies (Abell 1958, Zwicky et al. 1961–68) were constructed by visual inspection of the Palomar Observatory Sky Survey plates. Cluster catalogues have been used to find superclusters of galaxies (Oort 1983, Bahcall 1988, Einasto et al. 1994, 1997, 2001, Basilakos 2003).

A major problem in the use of Abell clusters of galaxies is the subjective character of the detection of clusters. This problem can be avoided if catalogues of galaxies of sufficient depth are available. Such catalogues are provided by the Las Campanas Redshift Survey (LCRS) (Shectman et al. 1996) and by the Early Data Release of the Sloan Digital Sky Survey (SDSS EDR) (Stoughton et al. 2002). These surveys contain data on galaxies in relatively thin slices of size of 1.5×90 degrees and of effective depth $z = 0.2$. Using the LCRS and the SDSS EDR it is possible to calculate two-dimensional density fields of galaxies and to detect groups and clusters of galaxies as density peaks of the field. Similarly it is possible to find superclusters of galaxies as large overdensity regions of the density field. Here I shall report results of the determination of the density fields of the LCRS and the SDSS EDR, and of the properties of clusters and superclusters of galaxies found from the density field. A more detailed description of our results is published elsewhere (Einasto et al. 2003a, 2003b), see also the web-site of Tartu Observatory (http://www.aai.ee).

Table 1. Data on SDSS EDR and LCRS galaxies, clusters and superclusters

Sample	DEC	RA	ΔRA	$N_{\rm gal}$	$N_{\rm DF}$	$N_{\rm LG}$	$N_{\rm ACO}$	$N_{\rm scl}$
SDSS.N	0°	190.2	90.5	15209	2868		22	24
SDSS.S	0°	23.2	65.5	11882	2287		16	16
LCRS	−3°	191.4	81.0	4065	1203	289	18	19
LCRS	−6°	189.8	77.9	2323	952	147	13	17
LCRS	−12°	191.4	81.1	4482	1266	276	11	15
LCRS	−39°	12.1	113.8	3922	1285	256	28	18
LCRS	−42°	12.2	112.5	4158	1216	265	19	14
LCRS	−45°	12.3	114.1	3753	1182	263	20	17

2. Observational data

The SDSS Early Data Release consists of two slices of about 2.5 degrees thick and $65 - 90$ degrees wide, centred on the celestial equator, one in the Northern and the other in the Southern Galactic hemisphere (Stoughton et al. 2002). We obtained from the SDSS Catalogue Archive Server the angular positions, Petrosian magnitudes, and other available data for all the EDR galaxies. From this general sample we extracted the Northern and Southern slice samples using the following criteria: the redshift interval $1000 \leq cz \leq 60000$ km s^{-1}, and the Petrosian r^*-magnitude interval $13.0 \leq r^* \leq 17.7$. The mean DEC, RA and RA intervals and the number of galaxies extracted N_{gal} are given in Table 1. The co-moving distances of galaxies were calculated using a cosmological model with the following parameters: the matter density $\Omega_m = 0.3$, the dark energy density $\Omega_\Lambda = 0.7$, the total density $\Omega_0 = \Omega_m + \Omega_\Lambda = 1.0$, all in units of the critical cosmological density (see Peacock 1999). With these parameters the limiting redshift $z_{lim} = 0.2$ corresponds to the co-moving distance $r_{lim} = 571\ h^{-1}$ Mpc. In calculating absolute magnitudes we used K-corrections and the correction for absorption in the Milky Way.

The LCRS (Shectman et al. 1996) is an optically selected galaxy redshift survey that extends to a redshift of 0.2 and covers six slices of width of 1.5 degrees, 3 slices are located in the Northern Galactic cap, and 3 in the Southern cap. The spectroscopy of the survey was carried out via a 50 or a 112 fibre multi-object spectrograph; therefore the selection criteria vary from field to field. The nominal apparent magnitude limits for the 50 fibre fields are $m_1 = 16.0 \leq R \leq m_2 = 17.3$, and for the 112 fibre fields $m_1 = 15 \leq R \leq m_2 = 17.7$. The data on the LCRS slices are given in Table 1.

We also use the sample of rich clusters of galaxies by Abell (1958) and Abell et al. (1989) (hereafter Abell clusters), compiled by Andernach & Tago (1998), with redshifts up to $z = 0.13$. This sample was described in detail by Einasto et al. (2001), where an updated supercluster catalogue of Abell clusters was presented. Superclusters were identified as clusters of Abell clusters using a friend-of-friends

algorithm with a neighbourhood radius of 24 h^{-1} Mpc. For the LCRS we use also the catalogue of loose groups with at least 3 observed galaxies by Tucker et al. (2000).

3. Density field clusters

3.1. *The high-resolution density field of the SDSS*

We shall use the density field to find density enhancements – density field clusters, or shortly DF-clusters. The procedure consists of the following steps: (1) calculation of the distance, the absolute magnitude, and a weight factor for each galaxy of the sample; (2) calculation of rectangular coordinates of galaxies; (3) smoothing of the density field using an appropriate kernel and a smoothing length, and (4) finding clusters (density enhancements) in the field. When calculating the density field we regard every galaxy as a visible member of a density enhancement (group or cluster) within the visible range of absolute magnitudes, M_1 and M_2, corresponding to the observational window of apparent magnitudes at the distance of the galaxy. This assumption is based on observations of nearby galaxies, which indicate that practically all giant galaxies are surrounded by dwarf companions, like our own Galaxy or the M31.

The expected number and luminosities of faint galaxies outside the visibility window is calculated using the Schechter (1976) luminosity function with parameters given by Einasto et al. (2003a, 2003b). When calculating of the total luminosity of the group, we have encountered two selection effects. When using Schechter parameters found with conventional methods we multiply the luminosity of the observed galaxy by a weight which takes statistically into account all galaxies outside the visibility window. As we shall see below, on large distances faint groups and clusters of galaxies are completely missed since they contain no objects inside the visibility window. To take these galaxies into account their luminosity is added to the luminosity of visible groups and clusters. As a result the visible groups and clusters become too bright, but the summed luminosity of all groups and clusters at a given distance is correct. Thus in this case we get correct properties of superclusters of galaxies, which are defined as large overdensity regions. To get correct properties for individual groups and clusters we have used another set of Schechter parameters which do not add the luminosity of completely invisible groups to the luminosity of visible ones. With this set of parameters we have calculated all properties of DF-clusters, their luminosity distribution etc.

As an example, we plot in Fig. 1 number-density and luminous-density weights for the luminosity function which yields correct properties for individual DF-clusters (for the Northern slice). Also we show the luminosities of galaxies L_{obs}, and the expected total luminosities L_{tot}. The luminosities are expressed in the units of 10^{10} Solar luminosities. We see that the number-density weights W_N rise monotonically with the increasing distance from the observer, whereas the luminous-density weights W_L rise also toward very small distances. This is due to the influence of bright galaxies outside the observational window, which are not numerous, but are

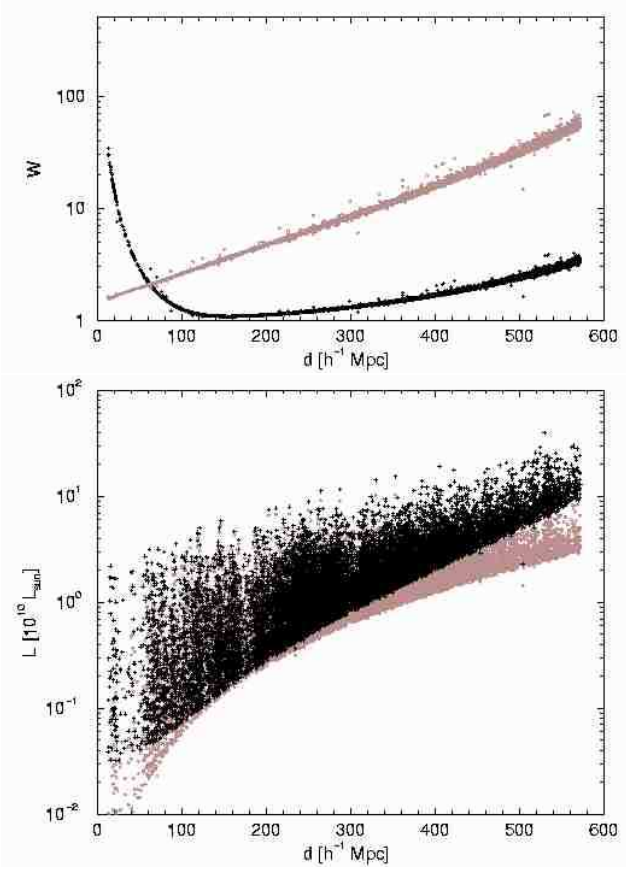

Figure 1. The upper panel shows the weights as a function of distance. Grey symbols indicate the number-density weights, black symbols – the luminous-density weights. The lower panel plots luminosities of galaxies as a function of distance. Grey circles mark luminosities of observed galaxies, black symbols mark total luminosities, corrected for the unobservable part of the luminosity range. Here we use the luminosity function parameters of set 1, which yield better DF-clusters.

very luminous.

To find the luminous-density field we calculated rectangular equatorial coordinates for all galaxies. The coordinates were rotated to obtain a situation where the new y-axis was oriented toward the average right ascension of each slice, and was rotated around the x-axis so as to force the average z-coordinate to be zero in order to minimise the projection effects. The SDSS slices are located around the celestial equator, thus the last rotation angle is in this case zero.

To calculate the density fields, we formed a grid of a cell size of 1 h^{-1} Mpc, and used only the $x, y-$coordinates. Ignoring the $z-$coordinate is equivalent to integrating over this coordinate, i.e. we find actually the projected density of the wedge. Finally the density field was smoothed using the Gaussian smoothing. To

find compact overdensity objects – the DF-clusters – we used a smoothing length of $0.8\ h^{-1}$ Mpc, this field is shown in Fig. 2. Since the thickness of the wedge increases with the distance from the observer, the number of DF-clusters per unit surface area also increases.

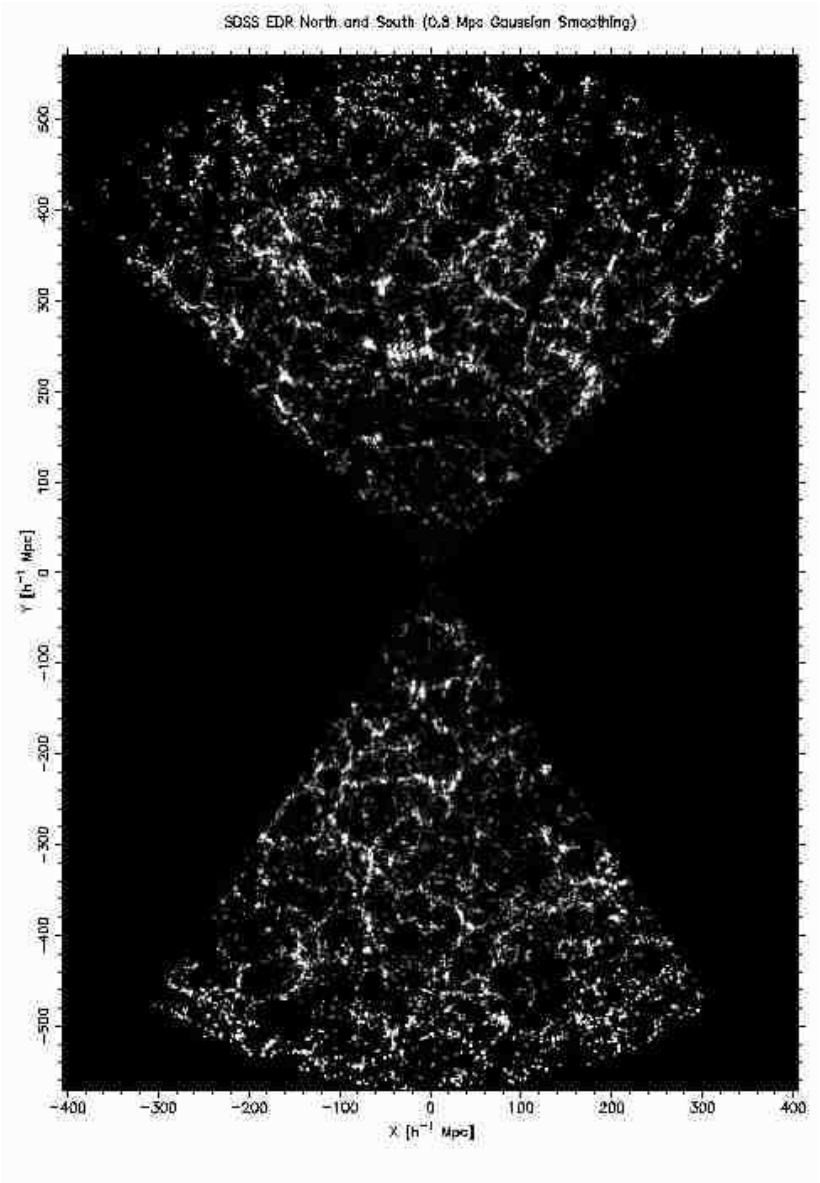

Figure 2. The density field of the SDSS EDR slices, smoothed with a Gaussian of $\sigma = 0.8\ h^{-1}$ Mpc dispersion.

3.2. *DF-clusters*

DF-clusters of galaxies were identified as peaks of the high-resolution density field. The total luminosity of a DF-cluster was derived by adding the luminosity densities of 5×5 cells centred at the cell with the highest luminosity density. This corresponds to the dispersion 0.8 h^{-1} Mpc used in smoothing. The luminosities were calculated in Solar luminosity units. We also calculated the density in units of the mean density, this relative density is used in Fig. 2 for plotting. A cluster was added to the list of DF-clusters if its luminosity L exceeded the threshold value $L_0 = 0.4\ 10^{10}\ L_\odot$, and its distance was in the interval $100 \leq d \leq 550\ h^{-1}$ Mpc. The total number of DF-clusters found is given in Table 1.

Now we look at some properties of DF-clusters. Fig. 3 shows the luminosities of DF-clusters as a function of the distance from the observer, d. The lowest luminosity clusters are seen only at distances $d \leq 150\ h^{-1}$ Mpc. There exists a well-defined lower limit of cluster luminosities at larger distances, the limit being linear in the $\log L - d$ plot. Such behaviour is expected, as at large distances an increasing fraction of clusters does not contain any galaxies bright enough to fall into the observational window of absolute magnitudes, $M_1 \ldots M_2$.

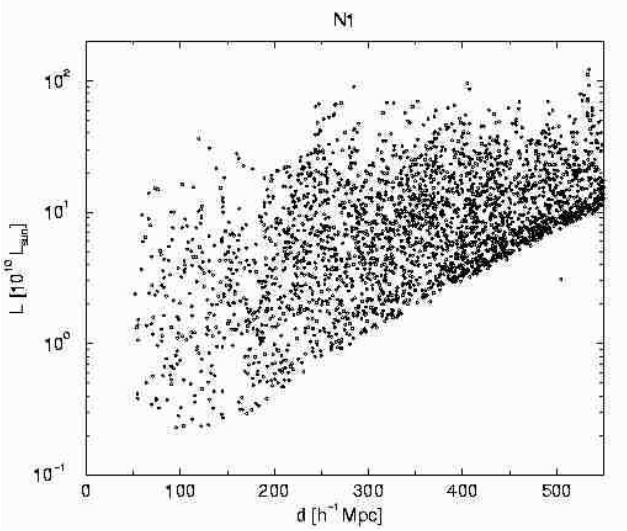

Figure 3. Luminosities of DF-clusters as a function of distance for the Northern slice, for the parameter set 1.

3.3. *The luminosity function of DF-clusters*

Now we calculate the integrated luminosity function of DF-clusters, i.e. the number of DF-clusters per unit volume exceeding a given luminosity L. Fig. 3 shows that only very bright DF-clusters are observable over the whole depth of our

samples. The estimated total number of fainter clusters can be found by multiplying the observed number of clusters by a weighting factor $(d_{lim}/d_L)^3$, where $d_{lim} = 550\ h^{-1}$ Mpc is the limiting distance used in compiling the DF-cluster sample, and d_L is the largest distance where clusters of luminosity L are seen. The luminosity functions of DF-clusters for both the SDSS samples are shown in Fig. 4.

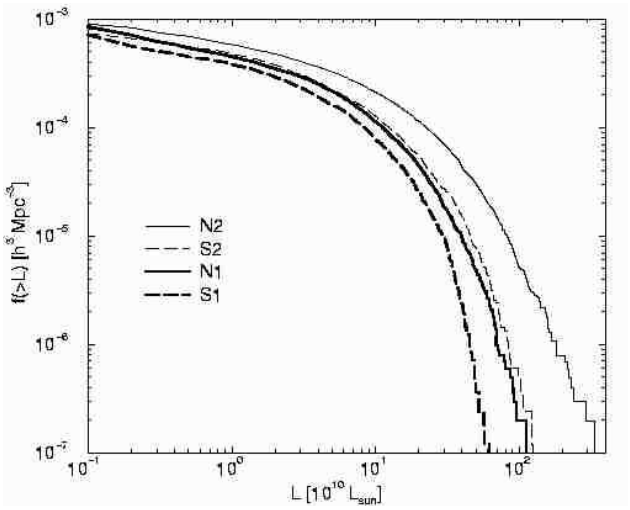

Figure 4. Integrated luminosity functions of DF-clusters for the parameter sets 1 and 2.

We see that the luminosity functions span over 3 orders in luminosity and almost 4 orders in spatial density. The bright DF-clusters are the density field equivalents of rich clusters of the Abell class, fainter DF-clusters correspond to groups of galaxies. The broad coverage of luminosities shows that the SDSS sample is well suited for determining the luminosity function from observations. The number of bright clusters is much larger for the parameter set 2. As discussed above, this is due to the overcorrection of cluster luminosities – particularly at large distances – to compensate for non-detected faint clusters. Thus we believe that the function for the parameter set 1 corresponds better to reality. Our results also show that the Northern SDSS sample has a larger number of luminous DF-clusters than does the Southern sample.

3.4. *Environmental effects in the distribution of DF-clusters*

We can use the density found with the 10 h^{-1} Mpc smoothing as an environmental parameter to describe the global density in the supercluster environment of clusters. We calculated this global density ϱ_0 (in units of the mean density of the low-resolution density field) for all the DF-clusters. Fig. 5 shows the luminosity of DF-clusters as a function of the global density ϱ_0. There is a clear correlation

between the luminosity of DF-clusters and their environmental density. Luminous clusters are predominantly located in high-density regions, and low-luminosity clusters in low-density regions. This tendency is seen also visually in the colour version of Fig. 2 (see Einasto et al. 2003a and the web-site of Tartu Observatory). Here densities are colour-coded, and we see that small clusters in voids have blue colours which indicate medium and small densities, whereas rich clusters having red colours populate dominantly the central high-density regions of superclusters.

For comparison we show in Fig. 6 the masses of clusters in numerical simulations as a function of the global relative density. The numerical model was calculated for a box of size 200 h^{-1} Mpc, using the cosmological parameters: $\Omega_m = 0.3$, $\Omega_\Lambda = 0.7$. The masses of clusters are characterised by the number of particles in clusters, N. We see that in high-density environments most massive clusters are more than a hundred times more massive than in low-density environments. The contrast is larger than that found for the observed DF-clusters. Probably this is due to a higher mass resolution in numerical simulations.

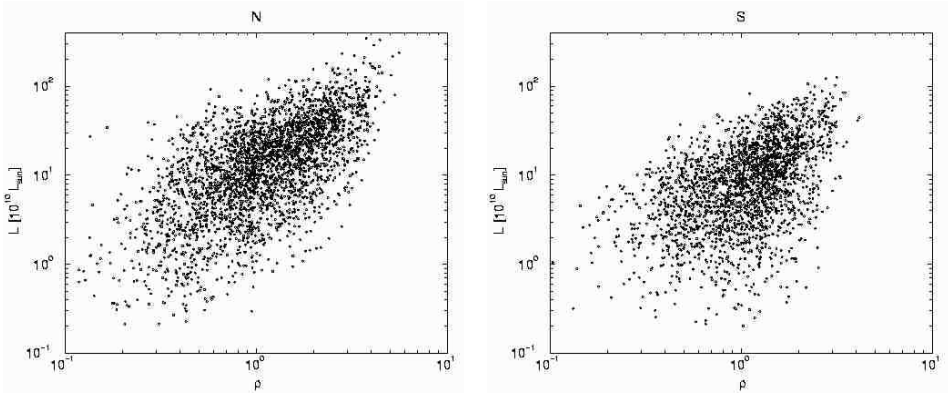

Figure 5. The luminosities of DF-clusters as a function of the global relative density ϱ_0. The left panel shows the Northern slice, the right panel the Southern slice.

Fig. 5 shows also that the Northern sample has much more luminous clusters than the Southern sample. This result confirms the presence of a difference between the structure of Northern and Southern samples.

Fig. 7 shows the cluster luminosity functions of the Northern and Southern slices calculated separately for 4 global density intervals, $0 < \varrho_0 \leq 0.5$, $0.5 < \varrho_0 \leq 1.0$, $1.0 < \varrho_0 \leq 1.8$, and $1.8 < \varrho_0 \leq 10$, labelled in Fig. 7 as N0.0, N0.5, N1.0 and N1.8, for the Northern subsamples, and S0.0, S0.5, S1.0, S1.8 for the Southern ones. The functions were calculated for the luminosity function parameter set 1 (which yields an almost constant highest luminosity for the DF-clusters for various distances from the observer). We see that the luminosity functions depend very strongly on the global environment: the luminosity of the most luminous clusters in subsamples

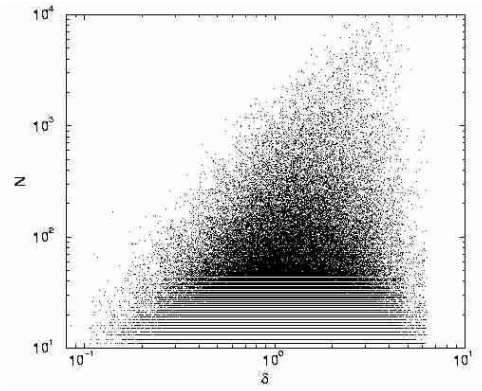

Figure 6. The masses of clusters in numerical simulation as a function of the global relative density ϱ_0.

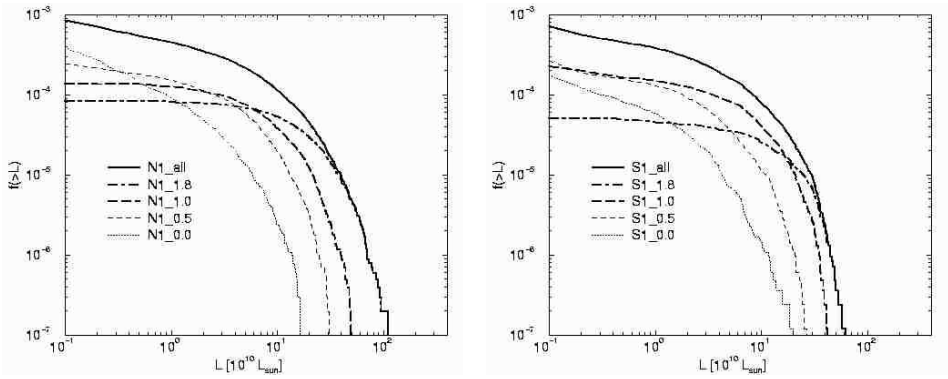

Figure 7. The integrated luminosity functions of the DF-clusters for various global relative density intervals ϱ_0. The left panel shows the Northern slice, the right panel – the Southern slice.

differs by a factor of 5 ± 2 (for a finer global density division the most luminous DF-clusters differ in luminosity even up to 10 times in extreme density regions). This difference is not statistical, due to different numbers of clusters, as these numbers are all of the same order.

4. Density field superclusters

4.1. *The supercluster catalogue*

Superclusters have been traditionally defined either as clusters of clusters of galaxies (Oort 1983, Bahcall 1988), using Abell clusters (Einasto et al. 1994, 1997, 2001), or as large and rich systems of galaxies (de Vaucouleurs 1953). In the present analysis we use the low-resolution density field of galaxies to find large overdensity regions which we call density field superclusters or for short DF-superclusters.

The compilation of the supercluster catalogue consists of three steps: (1) cal-

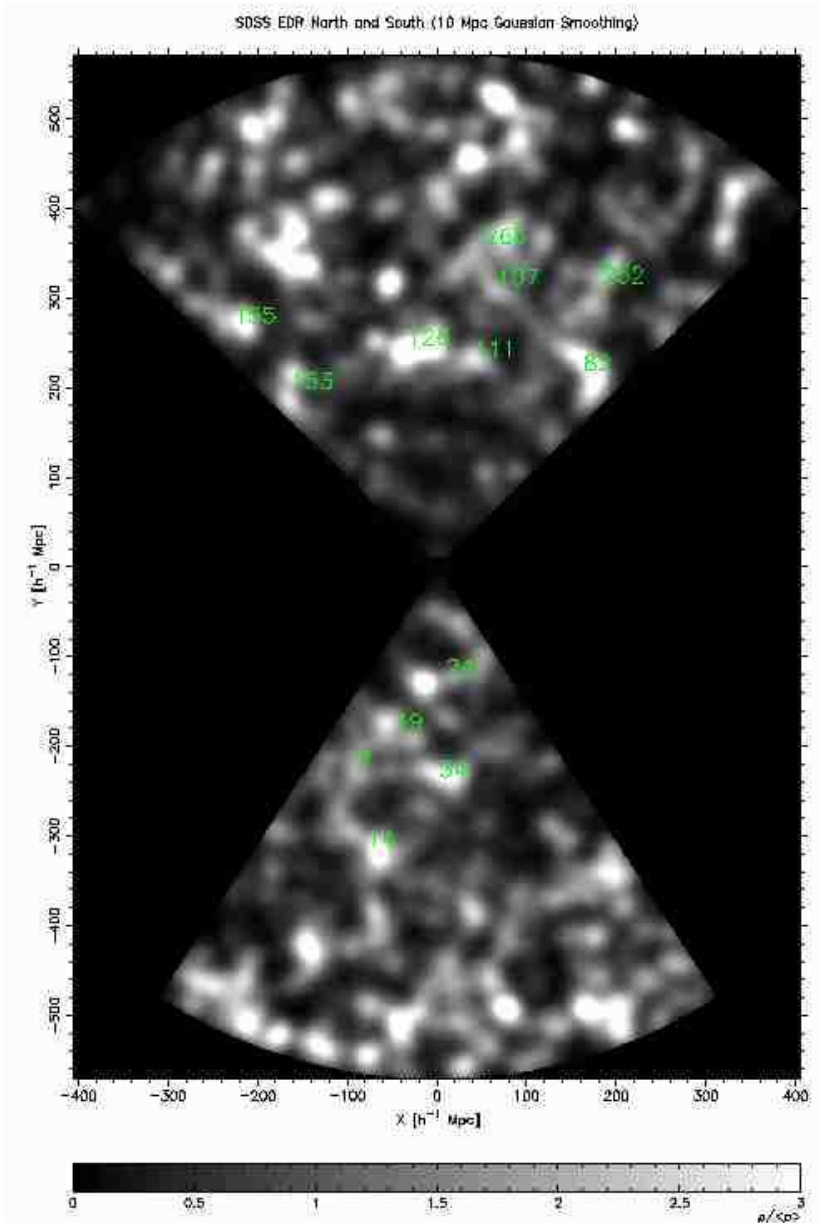

Figure 8. The density field of the SDSS EDR slices, smoothed with $\sigma = 10\ h^{-1}$ Mpc. The numbers denote Abell superclusters according to Einasto et al. (2001).

culating the density field, 2) finding the overdensity regions, and 3) determining the properties of the resulting superclusters. The density field was calculated as described above with one difference – in order to reduce the wedge-like volume of

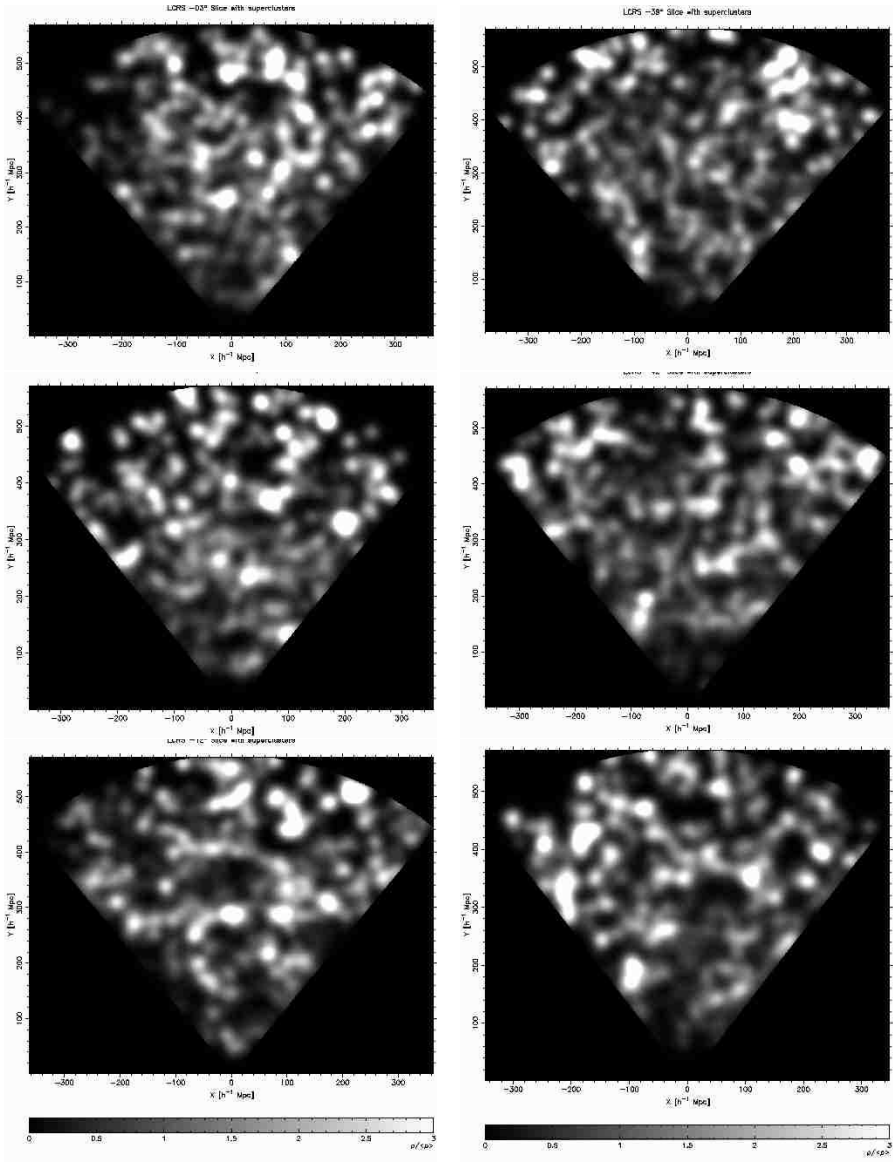

Figure 9. The density field of the LCRS slices smoothed with a $\sigma = 10\ h^{-1}$ Mpc Gaussian filter. The densities are reduced to a sheet of constant thickness.

slices to a sheet of uniform thickness we divided densities by the thickness of the slice at each particular distance. In this way the surface density of the field is on average independent of distance, and we can use a distance independent search for overdensity regions. The reduced density field for the Northern and Southern SDSS EDR slices is shown in Fig. 8. Fig. 9 shows the low-resolution density field of the

six sheets of the Las Campanas Redshift Survey. The field was calculated similarly to the low-density field of the Sloan Survey.

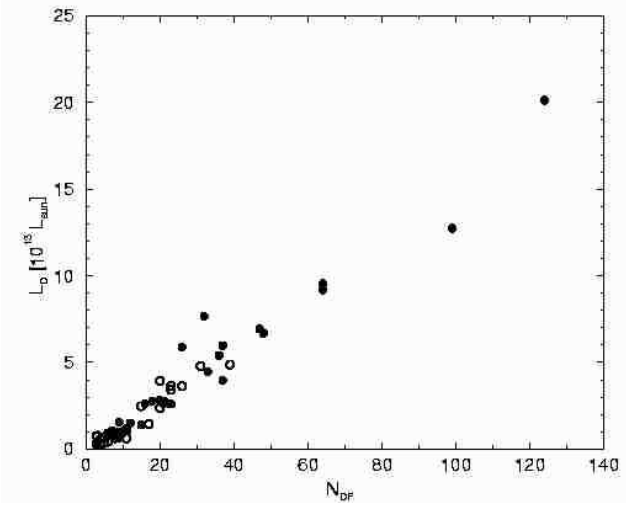

Figure 10. The total luminosities of the DF-superclusters versus the number of DF-clusters in a supercluster (supercluster richness). Filled circles: DF-superclusters which belong to the superclusters of Abell clusters, open circles: DF-superclusters that do not belong to the Abell superclusters.

Next we searched for connected high-density regions. To do so we need to fix the threshold density, ϱ_0, which divides the high- and low-density regions. This threshold density plays the same role as the neighbourhood radius used in the friends-of-friends (FoF) method to find clusters in galaxy samples and to find superclusters in cluster samples. To make a proper choice of the threshold density we calculated the number of superclusters, the area of the largest supercluster, and the maximum diameter of the largest supercluster as a function of the threshold density ϱ_0. This test shows that a proper value of the threshold density is $\varrho_0 = 1.8$ (we use relative densities here). In this case most superclusters are well separated, only one large supercluster consists of several density enhancements, which are separated at $\varrho_0 = 2.1$. Superclusters were found for the distance interval $100 \leq d \leq 550\ h^{-1}$ Mpc, with areas greater than 100 $(h^{-1}\,\mathrm{Mpc})^2$. The number of superclusters in the SDSS and LCRS slices is shown in Table 1.

We also calculated the observed total luminosity of a supercluster L_{obs} (the sum of the observed luminosities of the DF-clusters located within the boundaries of a supercluster), and the total luminosity of the supercluster L_{tot}. The total luminosity was calculated from the observed luminosity under the assumption that the vertical diameter of the supercluster is identical to the diameter in the plane of the slice. Using the spatial distribution of the DF-clusters we estimated also the morphological type of the supercluster.

4.2. *The fine structure of superclusters and voids*

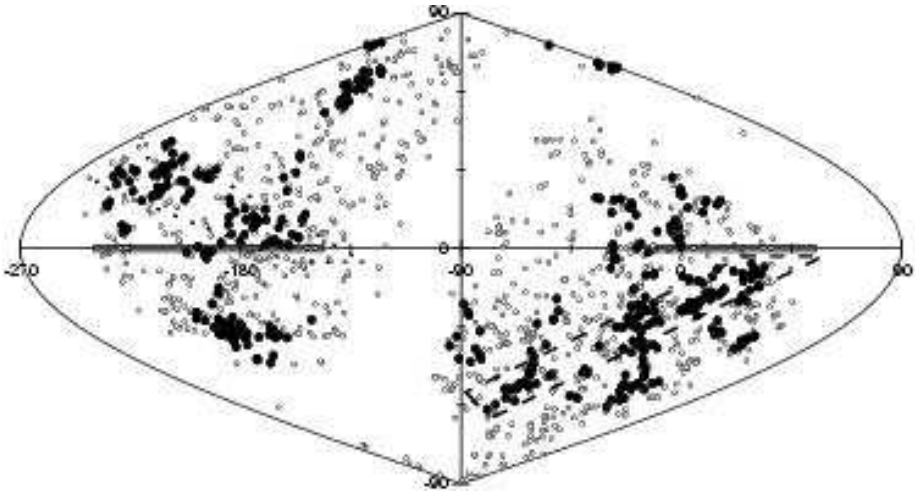

Figure 11. A view of Abell clusters in equatorial coordinates. Filled circles show the Abell clusters located in superclusters of richness 8 and more members, open circles mark the Abell clusters in less rich superclusters. The strips near the celestial equator mark the SDSS slices, the Northern slice is at the left side. The areas surrounded by dashed lines indicate regions where rich superclusters of the Dominant Supercluster Plane are located. The Galactic zone of avoidance is a S-shaped curve in equatorial coordinates.

The distribution of DF-clusters within DF-superclusters yields information on the internal structure of superclusters. A close inspection of Figs. 2 and 8 shows that superclusters have different internal structures: clusters may form a single filament, a branching system of filaments, or a more or less diffuse cloud of clusters. Most rich superclusters have a multi-filamentary morphology, poor superclusters consist usually of one cluster filament, or have a compact morphology without a clear filamentary system. Most superclusters are surrounded by faint systems of galaxies, either in the form of filaments or of a diffuse cloud of clusters.

In the SDSS and LCRS samples about $15 - 25\%$ of all DF-clusters are located in superclusters. Most DF-clusters outside superclusters also form filaments. Thus we come to the conclusion that there is no major difference in the shape of cluster systems in supercluster and in non-supercluster environments. This similarity of the structure within and outside superclusters is partly due to our formal procedure of defining superclusters; actually there is a continuous sequence of structures from single filaments to multiple filaments and superclusters. The difference is mainly in the luminosity of clusters. This observation can be interpreted as follows: clusters and cluster filaments in various environments are formed by similar density perturbations. Small-scale perturbations are modulated by large-scale perturbations which make clusters and their filaments richer in superclusters and poorer in large

voids between superclusters (see also Frisch et al. 1995).

Fig. 10 shows the total luminosities of superclusters versus their richnesses (the number of DF-clusters in a supercluster). This figure shows that those DF-superclusters that are also the Abell superclusters are more luminous and richer than the non-Abell DF-superclusters. Einasto et al. (2003b, 2003c, 2003d) showed, using the data on the Las Campanas loose groups (Tucker et al. 2000), that the loose groups in superclusters of Abell clusters are richer, more luminous, and more massive than the loose groups in systems that do not belong to Abell superclusters. This shows that the presence of rich (Abell) clusters is closely related to the properties of superclusters themselves.

Figs. 5 and 7 show that the Northern slice of the Sloan survey contains many very luminous DF-clusters, and in the Southern slice the most luminous clusters are less luminous. The number of rich superclusters in the Northern slice of the SDSS is also much higher than in the Southern slice. The distribution of Abell clusters on the celestial sphere is presented in Fig. 11. The regions of the SDSS EDR are marked by solid strips. The Northern slice lies in a region of space containing many rich superclusters. The $\pm 10^\circ$ zone around the celestial equator in the right ascension interval of the Northern slice contains 25 Abell superclusters in the catalogue by Einasto et al. (2001), among these, there are 5 very rich superclusters containing 7 or more Abell clusters. The $\pm 10^\circ$ zone around the Southern slice has 12 Abell superclusters, among which there is only one very rich system.

The discovery of large differences between the number and luminosity of clusters in different slices of surveys is one of main results of this study. We see that the number and richness of superclusters also varies in a similar manner. Evidently properties of clusters as well as of superclusters are influenced by density perturbations of very large scale.

5. Conclusions

- Galaxy systems have a similar shape in superclusters and voids: the dominant structural elements are single or multi-branching filaments. Massive superclusters have dominantly a multi-branching morphology; less massive superclusters have various morphologies, including compact, filamentary, multi-branching, and diffuse systems.
- Selection effects distort the distribution of clusters and superclusters in two different ways. If a cluster has at least one galaxy bright enough to be included into the redshift survey, then the total luminosity of the cluster can be restored supposing that the galaxy luminosity function can be applied for individual clusters. If the cluster has no bright galaxies, it is lost. A respective correction can be made only at supercluster scales.
- There exists a strong dependence of cluster properties on the density of the large-scale environment: clusters located in high-density environments are a factor of 5 ± 2 more luminous than clusters in low-density environments,

and in extreme environmental density regions the difference is even larger.
- There exists a large difference between the properties of clusters and superclusters in the Northern and Southern slices of the SDSS EDR survey: the clusters and superclusters in the Northern slice are more luminous than those in the Southern slice by a factor of 2. This difference may be due to differences in the location of slices with respect to the very large-scale environment.

Acknowledgements

I thank Maret Einasto, Gert Hütsi, Enn Saar, Douglas Tucker, Volker Müller, Pekka Heinämäki, Heinz Andernach and Erik Tago for collaboration and for the permission to use our common results in this review talk. The present study was supported by the Estonian Science Foundation grant ETF 4695, and by grant TO 0060058S98. I thank Fermilab and the Astrophysikalisches Institut Potsdam (DFG-grant 436 EST 17/2/01) where part of this study was performed, for hospitality.

References

1. Abell, G., 1958, ApJS, 3, 211
2. Abell, G., Corwin, H. & Olowin, R., 1989, ApJS, 70, 1
3. Andernach, H. & Tago, E., 1998, in *Large Scale Structure: Tracks and Traces*, eds. V. Müller, S. Gottlöber, J.P. Mücket & J. Wambsganss, World Scientific, Singapore, p. 147
4. Bahcall, N., 1988, ARAA, 26, 631
5. Basilakos, S., 2003, MNRAS 344, 602
6. de Vaucouleurs, G., 1953, AJ, 58, 30
7. Einasto, J., Einasto, M., Hütsi, G. et al. 2003b, A&A, 410, 425
8. Einasto, J., Hütsi, G., Einasto, M., et al. 2003a, A&A, 405, 425
9. Einasto, M., Einasto, J., Müller, V., Heinämäki, P. & Tucker, D. L., 2003c, A&A, 401, 851,
10. Einasto, M., Jaaniste, J., Einasto, J. et al. 2003d, A&A, 405, 821
11. Einasto, M., Einasto, J., Tago, E., Dalton, G. & Andernach, H., 1994, MNRAS, 269, 301
12. Einasto, M., Einasto, J., Tago, E., Müller, V. & Andernach, H., 2001, AJ, 122, 2222
13. Einasto, M., Tago, E., Jaaniste, J., Einasto, J. & Andernach, H., 1997, A&A Suppl., 123, 119
14. Frisch, P., Einasto, J., Einasto, M. et al. 1995, A&A, 296, 611
15. Oort, J.H., 1983, ARAA, 21, 373
16. Peacock, J.A., 1999, Cosmological Physics (Cambridge: Cambridge University Press)
17. Schechter, P., 1976, ApJ, 203, 297
18. Shectman, S. A., Landy, S. D., Oemler, A., et al. 1996, ApJ, 470, 172
19. Stoughton, C., Lupton, R. H., Bernardi, M. et al. 2002, AJ, 123, 485
20. Tucker, D.L., Oemler, A.Jr., Hashimoto, Y. et al. 2000, ApJS, 130, 237
21. Zwicky, F., Wield, P., Herzog, E., Karpowicz, M. & Kowal, C.T. 1961–68, Catalogue of Galaxies and Clusters of Galaxies, 6 volumes. Pasadena, California Inst. Techn.